sciendo

POLISH MARITIME RESEARCH 2 (122) 2024 Vol. 31; pp. 92-98
10.2478/pomr-2024-0025

Auto-berthing Control for MSVs with a Time-based Generator under Actuator Faults: A Concise Neural Single-Parameter Approach

Liping Chen *

School of Ocean Information Engineering, Jimei University, Xiamen, 361024 China

* Corresponding author: *lpchen@jmu.edu.cn(L. Chen)*

ABSTRACT

In this paper, we study the control problem of auto-berthing marine surface vessels (MSVs) within a predefined, finite time in the restricted waters of a port, in the face of internal and external uncertain dynamics and actuator faults. We first use radial basis function neural networks to reconstruct the internal uncertainties of the system; then, using the minimum learning parameter method, we transform the weights of the neural networks, the external disturbances of the system, and the bias fault factors into an indirect single-parameter neural learning mode. We also apply a robust depth information adaptation technique to estimate the upper bound on the composite disturbances online. Dynamic surface control technology alleviates the burden of virtual control derivative calculations. Finite-time convergence of the system is guaranteed by a predetermined finite-time function based on a time-based generator (TBG). Based on these methods, we design a finite-time fault-tolerant auto-berthing control scheme based on TBG. The stability of the system is analysed based on Lyapunov stability theory. Finally, we verify the effectiveness of the proposed control scheme through simulation.

Keywords: Auto-berthing control; Time-based generator; Minimum learning parameter; Finite-time control; Concise neural single-parameter; Actuator faults

INTRODUCTION

In recent years, with the continuous development of the marine economy, the problem of auto-berthing control (ABC) of marine surface vessels (MSVs) has received widespread attention [1]. When MSVs undergo automatic berthing, the systems rely on the force and torque of the propeller and propulsion system to work together [2]. The development of automatic berthing technology has promoted the continuous deepening of research on vessel motion control. In the related field of port logistics management, the development of automatic berthing technology has been related to port utilisation, and is an important factor in promoting environmentally sustainable development [3,4]. With the increasing expansion and complexity of the global trade system, the requirements for efficiency in port operations in related industries are constantly increasing [5]. Traditional manual operation methods have certain limitations in terms of accuracy, efficiency and environmental friendliness. The issue of how to develop advanced automatic berthing technology for surface vessels has therefore become a hot topic for both academia and industry.

The complex dynamic process of the movement of MSVs is affected by uncertain dynamics caused by external disturbances, and these external interference factors pose a huge challenge to the stability and safety of vessels. UnpredicTable environmental factors not only increase the complexity of vessel motion control but also impose higher requirements on the steady-state performance of the vessel control system. In this context, the use of disturbance observers (DOs) has become an effective way to solve the problem of external disturbances. Xia et al. [6] and Yang et al. [7] designed passive observers and nonlinear DOs for a control scheme. Passive observers estimate and compensate for perturbations through dynamic input from the system itself [6], and this approach offers

significant advantages in regard to energy efficiency and system simplification. In contrast, a nonlinear DO has greater advantages in dealing with complex disturbance problems caused by the nonlinear characteristics of vessel dynamics [7], but can only handle slowly changing perturbations. To solve this problem, Meng et al. [8] developed an adaptive DO that could adapt to changes in the environment and system dynamics by adjusting the observer parameters in real time. This method enhanced the adaptability of the system and its robustness to unknown disturbances and parameter changes. Yu et al. [9] developed an FTDO to further improve the efficiency of disturbance reconstruction, which ensured that the system could accurately estimate and compensate for disturbances within a finite time. However, it should be pointed out that this was a control scheme designed by combining radial basis neural networks (NNs) with FTDO, and the problem of the huge computational load imposed by such a solution was not addressed.

In practical applications, the steady-state performance and transient response of a vessel control system are crucial. Finite time control (FTC) technology can ensure that high-precision control tasks are completed within strict time limits, which enables MSVs to achieve rapid and accurate state adjustment within a finite time. This technology can also enhance an MSV's adaptability and response speed to sudden disturbances. Zhu et al. [10] and Zhang et al. [11] developed finite-time control schemes under internal and external uncertain dynamics. However, the introduction of NN technology increases the computational load of the system, and an indirect NN approximation scheme is more closely aligned with the actual needs of the application. Meng et al. [12] and Deng et al. [13] aimed to reduce the computational load of the system by introducing minimum learning parameter (MLP) technology. Ma et al. [14] developed an error-driving function to compensate for the control accuracy loss in norm calculation reported in [12] and [13]. However, this scheme did not have finite-time convergence characteristics. In addition, most of the studies described above did not consider limitations due to actuator faults.

Inspired by the above work, we develop a TBG-based predefined finite-time ABC scheme under actuator failure. The main contributions of this article are as follows:

(1) We solve the actuator fault problem in the ABC problem for the first time. Unlike the authors of [11,14], we consider the limitations arising from actuator faults by considering dynamic uncertainties and external disturbances. Unlike the studies in [12][17], the control scheme designed in this paper actively compensates for the loss-of-effectiveness (LOE) fault factor of the system.
(2) We integrate MLP with NNs and deep information robust adaptive technology to integrate the system's fault factors, external disturbances, and NN weights into a simple neural single-parameter form. Compared with [9][16], the processing method proposed in this paper reduces the system's computing load more effectively. Moreover, the designed scheme is concise and easy to apply in actual projects.
(3) We develop a novel FTC scheme. Unlike in [8][10], no additional proportional or differential terms are added to the structure of the control law; this ensures the conciseness of the controller structure and compensates for the loss of control accuracy in norm calculation.

PROBLEM FORMULATION AND PRELIMINARIES

PROBLEM FORMULATION

In general, a mathematical model for MSVs can be expressed as [18]:

$$\begin{cases} \dot{x} = u\cos(\psi) - v\sin(\psi) \\ \dot{y} = u\sin(\psi) + v\cos(\psi) \\ \dot{\psi} = r \end{cases} \tag{1}$$

$$\begin{cases} \dot{u} = f_u(v) + \frac{1}{m_{11}}(F_{\tau_u} + F_{d_u}) \\ \dot{v} = f_v(v) + \frac{1}{m_{22}}(F_{\tau_v} + F_{d_v}) \\ \dot{r} = f_r(v) + \frac{1}{m_{33}}(F_{\tau_r} + F_{d_r}) \end{cases} \tag{2}$$

where x, y, ψ represent the position and course angle of the MSV, respectively; u, v, r represent the surge velocity, sway velocity and yaw velocity, respectively; $f_u(v) = \frac{1}{m_{11}}(m_{22}ur - d_{11}u - d_u|u|u)$, $f_v(v) = \frac{1}{m_{22}}(-m_{11}ur - d_{22}v - d_v|v|v)$, $f_r(v) = \frac{1}{m_{33}}[(m_{11} - m_{22})uv - d_{33}u - d_r|r|r]$ are nonlinear dynamics; m_{11}, m_{22}, $m_{33}$are inertial masses; F_{d_u}, F_{d_v}, F_{d_r} represent external interference items; and F_{τ_u}, F_{τ_v}, F_{τ_r} represent control inputs subject to actuator fault constraints. Two types of actuator faults, known as LOE faults and bias faults, are considered in this work. The specific mathematical expressions for these are as follows [15]:

$$\begin{cases} F_{\tau_u} = F_{\rho_u}\tau_u + F_{\partial_u} \\ F_{\tau_v} = F_{\rho_v}\tau_v + F_{\partial_v} \\ F_{\tau_r} = F_{\rho_r}\tau_r + F_{\partial_r} \end{cases} \tag{3}$$

where τ_u, τ_v and τ_r represent control inputs; $0 < F_{\rho_u} < 1$, $0 < F_{\rho_v} < 1$, $0 < F_{\rho_r} < 1$ are LOE faults; and $F_{\partial_u} \neq 0$, $F_{\partial_v} \neq 0$, $F_{\partial_r} \neq 0$ are bias faults.

Assumption 1: $f_i(v)$, $i = (u, v, r)$ are unknown. Interference items outside the system external interference F_{d_i}, $i = (u, v, r)$ are unknown and bounded. That is, there are unknown positive constants θ_i, such that F_{d_i} satisfies $|F_{d_i}| \leq \theta_i$.

Assumption 2: A reference trajectory x_d, y_d, ψ_d, $\dot{x}_d$, $\dot{y}_d$, $\dot{\psi}_d$, $\ddot{x}_d$, $\ddot{y}_d$, $\ddot{\psi}_d$ is available.

PREDEFINED FINITE-TIME FUNCTION WITH TBG

TBG is a nonlinear time-related function whose initial and final values satisfy specific constraints. For the following

properties, if they are assigned (t^*) , the function can be called TBG [19].

(1) $[t^*(0)] = 1$, (t^*), $(\dot{t}^*)$, $(\ddot{t}^*)$ are continuous and bounded.
(2) $(t^*) = 1$ for $\forall t^* > \beta$, where β is the predefined setting time.
(3) The first and second derivatives of (t^*) exist, and are continuously decreasing for $\forall t^* \in [0, \beta]$.

The following are some clear examples of (t^*):

$$(t^*) = \begin{cases} \left[\frac{\beta - t^*}{\beta}\right]^p (p \geq 2) t^* < \beta \\ 0 \qquad\qquad t^* > \beta \end{cases} \tag{4}$$

$$(t^*) = \begin{cases} \left[\frac{\beta - t^*}{\beta}\right]^p e^{-t^*} (p \geq 2) t^* < \beta \\ 0 \qquad\qquad t^* > \beta \end{cases} \tag{5}$$

$$(t^*) = \begin{cases} \left[\frac{\beta - t^*}{\beta}\right]^p \lambda(t^*) (p \geq 2) t^* < \beta \\ 0 \qquad\qquad t^* > \beta \end{cases} \tag{6}$$

where $\lambda(t^*)$ is a continuous and non-increasing time-dependent function, and $\lambda(0) = 1$. $\lambda(t^*)$ is second-order differentiable. In addition, the function itself and its first and second derivatives are bounded.

According to the nature of TBG, we constructed the predefined finite-time function with TBG as follows:

$$\pi(t^*) = [(1-\sigma)(t^*) + \sigma]^{-1} \tag{7}$$

where $\sigma \in (0,1)$ is a positive definite design parameter.

Lemma 1 A predefined finite-time function with TBG has the following properties:

(1) $\pi(t^*)$ and $\dot{\pi}(t^*)$ are continuously differentiable and bounded. $\ddot{\pi}(t^*)$ is continuous and bounded.
(2) For all $t^* \in [0, \beta]$, $\pi(t^*)$ is a strictly increasing function.
(3) Let $\omega = \dot{\pi}(t^*)\ \pi^{-1}(t^*)$, where $\omega > 0$ and its derivative is continuous and bounded.

CONTROL DESIGN AND STABILITY ANALYSIS

First, we define the tracking error as follows

$$\begin{bmatrix} x_e \\ y_e \\ \psi_e \end{bmatrix} = \begin{bmatrix} x - x_d \\ y - y_d \\ \psi - \psi_d \end{bmatrix} \tag{8}$$

where x_d, y_d are the reference positions of the system, and ψ_d is the reference heading.

According to the finite-time function $\pi(t^*)$, the tracking error in (8) is converted as follows

$$\begin{cases} \tilde{x} = \pi_x x_e \\ \tilde{y} = \pi_y y_e \\ \tilde{\psi} = \pi_\psi \psi_e \end{cases} \tag{9}$$

Taking the time derivative of Eq. (9), we obtain

$$\begin{cases} \dot{\tilde{x}} = \dot{\pi}_x x_e + \pi_x(\dot{x} - \dot{x}_d) = \pi_x[\omega_x x_e + u\cos(\psi) - v\sin(\psi)] \\ \dot{\tilde{y}} = \dot{\pi}_y y_e + \pi_y(\dot{y} - \dot{y}_d) = \pi_y[\omega_y y_e + u\sin(\psi) + v\cos(\psi)] \\ \dot{\tilde{\psi}} = \dot{\pi}_\psi \psi_e + \pi_\psi(\dot{\psi} - \dot{\psi}_d) = \pi_\psi[\omega_\psi \psi_e + r] \end{cases} \tag{10}$$

Based on Eq. (10), the virtual control law is designed as follows:

$$\begin{cases} \delta_u = \cos^{-1}(\psi)[-\phi_1 x_e - \omega_x x_e + v\sin(\psi)] \\ \delta_v = \cos^{-1}(\psi)[-\phi_2 y_e - \omega_y y_e - u\sin(\psi)] \\ \delta_r = -\phi_3 \psi_e - \omega_\psi \psi_e \end{cases} \tag{11}$$

where ϕ_1, ϕ_2, ϕ_3 are positive definite design parameters.

The structural velocity tracking error is as follows:

$$\begin{bmatrix} u_e \\ v_e \\ r_e \end{bmatrix} = \begin{bmatrix} u - \hat{\delta}_u \\ v - \hat{\delta}_v \\ r - \hat{\delta}_r \end{bmatrix} \tag{12}$$

where $\hat{\delta}_u$, $\hat{\delta}_v$, $\hat{\delta}_r$ are the approximate values of virtual control after dynamic surface filtering. The specific form of the dynamic surface is as follows:

$$\begin{cases} \mu_1 \dot{\hat{\delta}}_u + \hat{\delta}_u = \delta_u \\ \mu_2 \dot{\hat{\delta}}_v + \hat{\delta}_v = \delta_v \\ \mu_3 \dot{\hat{\delta}}_r + \hat{\delta}_r = \delta_r \end{cases} \tag{13}$$

where μ_1, μ_2, μ_3 are positive definite filter parameters.

According to the finite-time function $\pi(t^*)$, the tracking error in Eq. (12) is converted as follows:

$$\begin{cases} \tilde{u} = \pi_u u_e \\ \tilde{v} = \pi_v v_e \\ \tilde{r} = \pi_r r_e \end{cases} \tag{14}$$

Taking the time derivative of Eq. (14), we obtain:

$$\begin{cases} \dot{\tilde{u}} = \dot{\pi}_u u_e + \pi_u(\dot{u} - \dot{\hat{\delta}}_u) = \pi_u\left[\omega_u u_e + f_u(v) + \frac{1}{m_{11}}(F_{\tau_u} + F_{d_u}) - \dot{\hat{\delta}}_u\right] \\ \dot{\tilde{v}} = \dot{\pi}_v v_e + \pi_v(\dot{v} - \dot{\hat{\delta}}_v) = \pi_v\left[\omega_v v_e + f_v(v) + \frac{1}{m_{22}}(F_{\tau_v} + F_{d_v}) - \dot{\hat{\delta}}_v\right] \\ \dot{\tilde{r}} = \dot{\pi}_r r_e + \pi_r(\dot{r} - \dot{\hat{\delta}}_r) = \pi_r\left[\omega_r r_e + f_r(v) + \frac{1}{m_{33}}(F_{\tau_r} + F_{d_r}) - \dot{\hat{\delta}}_r\right] \end{cases} \tag{15}$$

where $f_u(v)$, $f_v(v)$, $f_r(v)$ are unmeasurable. We use RBFNNs to reconstruct it. The specific process is as follows:

$$\begin{cases} f_u(v) = W_u^{\mathrm{T}} S_u(v) + \varepsilon_u \\ f_v(v) = W_v^{\mathrm{T}} S_v(v) + \varepsilon_v \\ f_r(v) = W_r^{\mathrm{T}} S_r(v) + \varepsilon_r \end{cases} \tag{16}$$

where v is the input vector of the NNs; $S_u(v)$, $S_v(v)$, $S_r(v)$ are central functions; and W_u^{T}, W_v^{T}, W_r^{T} are the weights of the NNs.

The Lyapunov function is constructed as follows

$$L_v = \frac{1}{2}\tilde{x}^2 + \frac{1}{2}\tilde{y}^2 + \frac{1}{2}\tilde{\psi}^2 + \frac{1}{2}\tilde{u}^2 + \frac{1}{2}\tilde{v}^2 + \frac{1}{2}\tilde{r}^2 \tag{17}$$

From the time derivative of Eq. (17), we have:

$$\begin{aligned} \dot{L}_v = {} & -\phi_1 \pi_x^{\,2} x_e^{\,2} - \phi_2 \pi_y^{\,2} y_e^{\,2} - \phi_3 \pi_\psi^{\,2} \psi_e^{\,2} + \\ & u_e \pi_u^{\,2} \left[x_e \pi_x^{\,2} \cos(\psi) + \omega_u u_e + f_u(v) + \frac{1}{m_{11}}(F_{\tau_u} + F_{d_u}) - \dot{\hat{\delta}}_u \right] + \\ & v_e \pi_v^{\,2} \left[y_e \pi_y^{\,2} \cos(\psi) + \omega_v v_e + f_v(v) + \frac{1}{m_{22}}(F_{\tau_v} + F_{d_v}) - \dot{\hat{\delta}}_v \right] + \\ & r_e \pi_r^{\,2} \left[\psi_e r_e \pi_\psi^{\,2} + \omega_r r_e + f_r(v) + \frac{1}{m_{33}}(F_{\tau_r} + F_{d_r}) - \dot{\hat{\delta}}_r \right] \end{aligned} \tag{18}$$

Substituting Eqs. (3) and (16) into Eq. (18), and combining the MLP technology, we obtain

$$\begin{aligned} \dot{L}_v = {} & -\phi_1 \pi_x^{\,2} x_e^{\,2} - \phi_2 \pi_y^{\,2} y_e^{\,2} - \phi_3 \pi_\psi^{\,2} \psi_e^{\,2} + u_e \pi_u^{\,2} P_u + u_e \pi_u^{\,2} F_{\rho_u} \tau_u + \\ & v_e \pi_v^{\,2} P_v + v_e \pi_v^{\,2} F_{\rho_v} \tau_v + r_e \pi_r^{\,2} P_r + r_e \pi_r^{\,2} F_{\rho_r} \tau_r \end{aligned} \tag{19}$$

where

$$P_u = x_e \pi_x^{\,2} \cos(\psi) + \omega_u u_e + W_u^{\mathrm{T}} S_u(v) + \varepsilon_u + m_{11}^{-1} F_{\partial_u} + m_{11}^{-1} F_{d_u} - \dot{\hat{\delta}}_u,$$

$$P_v = y_e \pi_y^{\,2} \cos(\psi) + \omega_v v_e + W_v^{\mathrm{T}} S_v(v) + \varepsilon_v + m_{22}^{-1} F_{\partial_v} + m_{22}^{-1} F_{d_v} - \dot{\hat{\delta}}_v,$$

$$P_r = \psi_e \pi_\psi^{\,2} + \omega_r r_e + W_r^{\mathrm{T}} S_r(v) + \varepsilon_r + m_{33}^{-1} F_{\partial_r} + m_{33}^{-1} F_{d_r} - \dot{\hat{\delta}}_r.$$

and

$$\begin{cases} ||P_u|| \le |x_e| \left| \pi_x^{\,2} \cos(\psi) \right| + |\omega_u| |u_e| + ||W_u^{\mathrm{T}}|| \, ||S_u(v)|| + \\ \quad \left| \varepsilon_u + m_{11}^{-1} F_{\partial_u} + m_{11}^{-1} F_{d_u} - \dot{\hat{\delta}}_u \right| \\ ||P_v|| \le |y_e| \left| \pi_y^{\,2} \cos(\psi) \right| + |\omega_v| |v_e| + ||W_v^{\mathrm{T}}|| \, ||S_v(v)|| + \\ \quad \left| \varepsilon_v + m_{22}^{-1} F_{\partial_v} + m_{22}^{-1} F_{d_v} - \dot{\hat{\delta}}_v \right| \\ ||P_r|| \le |\psi_e| \left| \pi_\psi^{\,2} \right| + |\omega_r| |r_e| + ||W_r^{\mathrm{T}}|| \, ||S_r(v)|| + \\ \quad \left| \varepsilon_r + m_{33}^{-1} F_{\partial_r} + m_{33}^{-1} F_{d_r} - \dot{\hat{\delta}}_r \right| \end{cases} \tag{20}$$

Then, Eq. (18) becomes

$$\begin{aligned} \dot{L}_v \le {} & -\phi_1 \pi_x^{\,2} x_e^{\,2} - \phi_2 \pi_y^{\,2} y_e^{\,2} - \phi_3 \pi_\psi^{\,2} \psi_e^{\,2} + u_e \pi_u^{\,2} \bar{\omega}_u \alpha_u + u_e \pi_u^{\,2} F_{\rho_u} \tau_u + \\ & v_e \pi_v^{\,2} \bar{\omega}_v \alpha_v + v_e \pi_v^{\,2} F_{\rho_v} \tau_v + r_e \pi_r^{\,2} \bar{\omega}_r \alpha_r + r_e \pi_r^{\,2} F_{\rho_r} \tau_r \end{aligned} \tag{21}$$

where

$$\bar{\omega}_u = \max\left\{ |\pi_x^{\,2} \cos(\psi)|, |\omega_u|, ||W_u^{\mathrm{T}}||, |\varepsilon_u + m_{11}^{-1} F_{\partial_u} + m_{11}^{-1} F_{d_u} - \dot{\hat{\delta}}_u| \right\},$$

$$\bar{\omega}_v = \max\left\{ |\pi_v^{\,2} \cos(\psi)|, |\omega_v|, ||W_v^{\mathrm{T}}||, |\varepsilon_v + m_{22}^{\,1} F_{\partial_v} + m_{22}^{-1} F_{d_v} - \dot{\hat{\delta}}_v| \right\},$$

$$\bar{\omega}_r = \max\left\{ |\pi_x^{\,2}|, |\omega_r|, ||W_r^{\mathrm{T}}||, 1 \right\}, \quad \alpha_u = |x_e| + |u_e| + ||S_u(v)|| + 1,$$

$$\alpha_v = |y_e| + |u_e| + ||S_v(v)|| + 1, \quad \alpha_r = |\psi_e| + |r_e| + ||S_r(v)|| + 1.$$

Based on this, the following control law is designed for the MSV automatic berthing system:

$$\begin{cases} \tau_u = -\phi_4 u_e \hat{\eta}_u - \hat{\bar{\omega}}_u \alpha_u u_e \\ \tau_v = -\phi_5 v_e \hat{\eta}_v - \hat{\bar{\omega}}_v \alpha_v v_e \\ \tau_r = -\phi_6 r_e \hat{\eta}_r - \hat{\bar{\omega}}_r \alpha_r r_e \end{cases} \tag{22}$$

and the adaptive law

$$\begin{cases} \dot{\hat{\eta}}_u = \gamma_{11}(\phi_4 u_e^{\,2} - \gamma_{12} \hat{\eta}_u) \\ \dot{\hat{\eta}}_v = \gamma_{21}(\phi_5 v_e^{\,2} - \gamma_{22} \hat{\eta}_v) \\ \dot{\hat{\eta}}_r = \gamma_{31}(\phi_6 r_e^{\,2} - \gamma_{32} \hat{\eta}_r) \end{cases} \tag{23}$$

$$\begin{cases} \dot{\hat{\bar{\omega}}}_u = \lambda_{11}(u_e^{\,2} \alpha_u - \lambda_{12} \hat{\bar{\omega}}_u) \\ \dot{\hat{\bar{\omega}}}_v = \lambda_{21}(v_e^{\,2} \alpha_v - \lambda_{22} \hat{\bar{\omega}}_v) \\ \dot{\hat{\bar{\omega}}}_r = \lambda_{31}(r_e^{\,2} \alpha_r - \lambda_{32} \hat{\bar{\omega}}_r) \end{cases} \tag{24}$$

where ϕ_4, ϕ_5, ϕ_6, γ_{11}, γ_{21}, γ_{31}, γ_{12}, γ_{22}, γ_{32}, λ_{11}, λ_{21}, λ_{31}, λ_{12}, λ_{22}, λ_{32} are positive definite parameters; $\hat{\eta}_u$, $\hat{\eta}_v$, $\hat{\eta}_r$, $\hat{\bar{\omega}}_u$, $\hat{\bar{\omega}}_v$, $\hat{\bar{\omega}}_r$ are estimates of η_u, η_v, η_r, $\bar{\omega}_u$, $\bar{\omega}_v$, $\bar{\omega}_r$; and $\eta_u = F_{\partial_u}^{-1}$, $\eta_v = F_{\partial_v}^{-1}$, $\eta_r = F_{\partial_r}^{-1}$.

We choose the following Lyapunov function for the closed-loop system:

$$\begin{aligned} M_v = {} & L_v + \frac{1}{2}\gamma_{11}^{-1} \pi_u^{\,2} F_{\rho_u} \tilde{\eta}_u^{\,2} + \frac{1}{2}\gamma_{21}^{-1} \pi_v^{\,2} F_{\rho_v} \tilde{\eta}_v^{\,2} + \frac{1}{2}\gamma_{31}^{-1} \pi_r^{\,2} F_{\rho_r} \tilde{\eta}_r^{\,2} + \\ & \frac{1}{2}\lambda_{11}^{-1} \pi_u^{\,2} F_{\rho_u} \tilde{\bar{\omega}}_u^{\,2} + \frac{1}{2}\lambda_{21}^{-1} \pi_v^{\,2} F_{\rho_v} \tilde{\bar{\omega}}_v^{\,2} + \frac{1}{2}\lambda_{31}^{-1} \pi_r^{\,2} F_{\rho_r} \tilde{\bar{\omega}}_r^{\,2} \end{aligned} \tag{25}$$

where $\tilde{\eta}_u = \eta_u - \hat{\eta}_u$, $\tilde{\eta}_v = \eta_v - \hat{\eta}_v$, $\tilde{\eta}_r = \eta_r - \hat{\eta}_r$, $\tilde{\bar{\omega}}_u = \bar{\omega}_u - \hat{\bar{\omega}}_u$, $\tilde{\bar{\omega}}_v = \bar{\omega}_v - \hat{\bar{\omega}}_v$, $\tilde{\bar{\omega}}_r = \bar{\omega}_r - \hat{\bar{\omega}}_r$ are estimation errors.

Taking the time derivative of Eq. (25), we get

$$\begin{aligned} \dot{M}_v \le {} & -\phi_1 \pi_x^{\,2} x_e^{\,2} - \phi_2 \pi_y^{\,2} y_e^{\,2} - \phi_3 \pi_\psi^{\,2} \psi_e^{\,2} + u_e \pi_u^{\,2} \bar{\omega}_u \alpha_u + u_e \pi_u^{\,2} F_{\rho_u} \tau_u + \\ & v_e \pi_v^{\,2} \bar{\omega}_v \alpha_v + v_e \pi_v^{\,2} F_{\rho_v} \tau_v + r_e \pi_r^{\,2} \bar{\omega}_r \alpha_r + r_e \pi_r^{\,2} F_{\rho_r} \tau_r - \\ & \gamma_{11}^{-1} \pi_u^{\,2} F_{\rho_u} \tilde{\eta}_u \dot{\hat{\eta}}_u - \gamma_{21}^{-1} \pi_v^{\,2} F_{\rho_v} \tilde{\eta}_v \dot{\hat{\eta}}_v - \gamma_{31}^{-1} \pi_r^{\,2} F_{\rho_r} \tilde{\eta}_r \dot{\hat{\eta}}_r - \\ & \lambda_{11}^{-1} \pi_u^{\,2} F_{\rho_u} \tilde{\bar{\omega}}_u \dot{\hat{\bar{\omega}}}_u - \lambda_{21}^{-1} \pi_v^{\,2} F_{\rho_v} \tilde{\bar{\omega}}_v \dot{\hat{\bar{\omega}}}_u - \lambda_{31}^{-1} \pi_r^{\,2} F_{\rho_r} \tilde{\bar{\omega}}_r \dot{\hat{\bar{\omega}}}_r \end{aligned} \tag{26}$$

Substituting Eqs. (22)–(24) into Eq. (26) gives

$$\dot{M}_v \le -\phi_1 \pi_x^{\,2} x_e^{\,2} - \phi_2 \pi_y^{\,2} y_e^{\,2} - \phi_3 \pi_\psi^{\,2} \psi_e^{\,2} - \phi_4 \pi_u^{\,2} u_e^{\,2} - \phi_5 \pi_v^{\,2} v_e^{\,2} - \phi_6 \pi_r^{\,2} r_e^{\,2} + \gamma_{12} \pi_u^{\,2} F_{\rho_u} \tilde{\eta}_u \hat{\eta}_u + \gamma_{22} \pi_v^{\,2} F_{\rho_v} \tilde{\eta}_v \hat{\eta}_v + \gamma_{32} \pi_r^{\,2} F_{\rho_r} \tilde{\eta}_r \hat{\eta}_r + \lambda_{12} \pi_u^{\,2} F_{\rho_u} \tilde{\bar{\omega}}_u \hat{\bar{\omega}}_u + \lambda_{22} \pi_v^{\,2} F_{\rho_v} \tilde{\bar{\omega}}_v \hat{\bar{\omega}}_v + \lambda_{32} \hat{\bar{\omega}}_r \pi_r^{\,2} F_{\rho_r} \tilde{\bar{\omega}}_r \tag{27}$$

From Young's inequality, we obtain

$$\begin{aligned} \dot{M}_v \le & -\phi_1 \pi_x^{\,2} x_e^{\,2} - \phi_2 \pi_y^{\,2} y_e^{\,2} - \phi_3 \pi_\psi^{\,2} \psi_e^{\,2} - \phi_4 \pi_u^{\,2} u_e^{\,2} - \phi_5 \pi_v^{\,2} v_e^{\,2} - \phi_6 \pi_r^{\,2} r_e^{\,2} - \tfrac{3}{4}\gamma_{12} \pi_u^{\,2} F_{\rho_u} \tilde{\eta}_u^{\,2} + \gamma_{12} F_{\rho_u} \pi_u^{\,2} - \tfrac{3}{4}\gamma_{22} \pi_v^{\,2} F_{\rho_v} \tilde{\eta}_v^{\,2} + \gamma_{22} F_{\rho_v} \pi_v^{\,2} - \tfrac{3}{4}\gamma_{32} \pi_r^{\,2} F_{\rho_r} \tilde{\eta}_r^{\,2} + \gamma_{32} F_{\rho_r} \pi_r^{\,2} - \\ & \tfrac{3}{4}\lambda_{12} \pi_u^{\,2} F_{\rho_u} \tilde{\bar{\omega}}_u^{\,2} + \lambda_{12} F_{\rho_u} \pi_u^{\,2} - \tfrac{3}{4}\lambda_{22} \pi_v^{\,2} F_{\rho_v} \tilde{\bar{\omega}}_v^{\,2} + \lambda_{22} F_{\rho_v} \pi_v^{\,2} - \\ & \tfrac{3}{4}\lambda_{32} \pi_r^{\,2} F_{\rho_r} \tilde{\bar{\omega}}_r^{\,2} + \lambda_{32} F_{\rho_r} \pi_r^{\,2} \\ \le & \kappa M_v + M_\kappa \end{aligned} \tag{28}$$

where

$\kappa = \min\{\phi_1, \phi_2, \phi_3, \phi_4, \phi_5, \phi_6, \frac{3}{4}\gamma_{12}, \frac{3}{4}\gamma_{22}, \frac{3}{4}\gamma_{32}, \frac{3}{4}\lambda_{12}, \frac{3}{4}\lambda_{22}, \frac{3}{4}\lambda_{32}\}$,

$M_\kappa = \gamma_{12} F_{\rho_u} \pi_u^{\,2} + \gamma_{22} F_{\rho_v} \pi_v^{\,2} + \gamma_{32} F_{\rho_r} \pi_r^{\,2} + \lambda_{12} F_{\rho_u} \pi_u^{\,2} + \lambda_{22} F_{\rho_v} \pi_v^{\,2} + \lambda_{32} F_{\rho_r} \pi_r^{\,2}$.

Theorem 1. According to the assumptions introduced in this article, the automatic berthing control strategy developed based on TBG can allow the MSV to reach the expected target position $(x_d, y_d, \psi_d)^{\mathrm{T}}$ within a finite time t^*, and all signals in the closed-loop system are bounded.

Proof: Solving Eq. (28) gives

$$M_v \le \left[M_v(0) - \frac{M_\kappa}{\kappa}\right] \exp(-\kappa t^*) + \frac{M_\kappa}{\kappa} \tag{29}$$

where $M_v(0)$ is the initial value of M_v.

Remark 1: From Eq. (40), we can see that M_v is bounded. Furthermore, according to Eqs. (17) and (25), we know that $\tilde{x}, \tilde{y}, \tilde{\psi}, \tilde{u}, \tilde{v}, \tilde{r}, \tilde{\eta}_u, \tilde{\eta}_v, \tilde{\eta}_r, \tilde{\bar{\omega}}_u, \tilde{\bar{\omega}}_v, \tilde{\bar{\omega}}_r$ are bounded. From the boundedness of $\tilde{x}, \tilde{y}, \tilde{\psi}, \tilde{u}, \tilde{v}, \tilde{r}$, we obtain the result that $x_e, y_e, \psi_e, u_e, v_e, r_e$ are bounded. Since u_e, v_e, r_e are bounded, then $\delta_u, \delta_v, \delta_r$ are bounded. Finally, by combining Assumption 1, Assumption 2 and the properties of TBG, it can be concluded that all signals in the closed-loop system are bounded.

Remark 2: From Eq. (29), $M_v \le \frac{M_\kappa}{\kappa} + M_v(0)$ can be obtained. Let $E_Z = (\tilde{x}, \tilde{y}, \tilde{\psi})^{\mathrm{T}}$; then $\frac{1}{2}||E_Z|| \le M_v \le \frac{M_\kappa}{\kappa} + M_v(0)$. It can then be shown that $E_Z \le \sqrt{2[\frac{M_\kappa}{\kappa} + M_v(0)]}$. If we let $\Phi = \sqrt{2[\frac{M_\kappa}{\kappa} + M_v(0)]}$, then $||E_p|| \le \Phi$. From Eq. (9), we can get

$$||E_p|| \le (1 - \sigma)\Phi(t^*) + \sigma\Phi \tag{30}$$

From the properties of ω, we know that when $t^* \ge T_v^*$, $\omega(0) = 0$ then $||E_p|| \le \sigma\Phi$. Hence, the MSV will reach the target location within a finite time T_v^*. Since ω is a TBG, the user can define the final value of the system and the predefined time T_v^*offline. Hence, T_v^* is predefined offline by the user. Finally, by combining **Remark 1** and **Remark 2**, **Theorem 1** is proved.

SIMULATIONS

For the simulations, we used the model vessel parameters reported in [20]. Their specific values are shown in Table 1. The external disturbance suffered by the system was set to $F_{d_u} = 0.2 + 0.015[\cos(-t) + \sin(-0.5t)]$, $F_{d_v} = 0.002[\sin(-0.15t) + 0.5\sin(-0.2t)]$, $F_{d_r} = 0.15 + 0.01[-\sin(3t)] - 2\cos(t)$, and the system's LOE faults were set to $F_{p_u} = 0.5 + 0.2\exp(-0.1t)$, $F_{p_v} = 0.3 + 0.5\exp(-0.2t)$, $F_{p_r} = 0.2 + 0.1\exp(-0.1t)$. The bias faults were set to $F_{\partial_u} = 0.1 + 0.5\cos(0.2t)$, $F_{\partial_v} = 0.2 + 0.3\cos(0.1t)$, $F_{\partial_r} = 0.3 + 0.25\sin(0.1t)$. The controller parameters were selected as $\phi = 0.2$, $\phi_2 = 0.1$, $\phi_3 = 0.8$, $\mu_1 = 0.01$, $\mu_2 = 0.01$, $\mu_3 = 0.02$, $\phi_4 = 0.5$, $\phi_5 = 1.2$, $\phi_6 = 0.6$, $\gamma_{11} = 0.3$, $\gamma_{21} = 0.5$, $\gamma_{31} = 0.1$, $\gamma_{12} = 0.03$, $\gamma_{22} = 0.07$, $\gamma_{32} = 0.01$, $\lambda_{11} = 1$, $\lambda_{21} = 3$, $\lambda_{31} = 2.1$, $\lambda_{12} = 0.01$, $\lambda_{22} = 0.05$, $\lambda_{32} = 0.01$.

Tab. 1. Model parameters

Parameter	Value	Parameter	Value	Parameter	Value
m_{11}	25.8	d_{11}	0.725	d_u	–1.33
m_{22}	33.8	d_{22}	0.89	d_v	–36.47
m_{33}	2.76	d_{33}	–1.9	d_r	–0.75

The results obtained from the simulation experiment are shown in Figs. 1 to 6. From Fig. 1, we see that in a complex environment where actuator faults and internal and external dynamic factors are affected, the MSV can successfully reach the established berth within a finite time. This proves that the proposed control scheme has excellent fault adaptability and efficient operation capabilities. Fig. 2 shows the evolution of the MSV's actual position and heading angle over time. It can be observed that the MSV's lateral position successfully reached the predetermined berth after 18 s, while a precise berthing was achieved after 133 s by finely adjusting the propeller power to alter its longitudinal position. In addition, the heading angle of the MSV eventually stabilised at 90° as time progressed, and no overshoot was experienced during the berthing process. This indicates the excellent steady-state performance of the system under this control scheme.

Fig. 3 shows that the system speeds reach sTable values at 10 s, 30 s, and 40 s, respectively. This indicates that the system can use the inherent inertia of the MSV to complete the remaining navigation operations, and demonstrates the excellent dynamic response characteristics of the system under this control scheme. Fig. 4 shows the changes in the system control input. The control input eventually stabilises to within a relatively small interval as time progresses, which verifies the effectiveness of the control strategy and the high level of adaptability of the

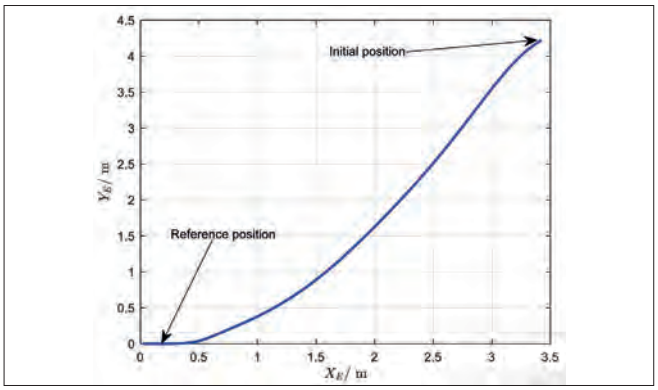

Fig. 1. Trajectory of the MSV in (x, y) -plant

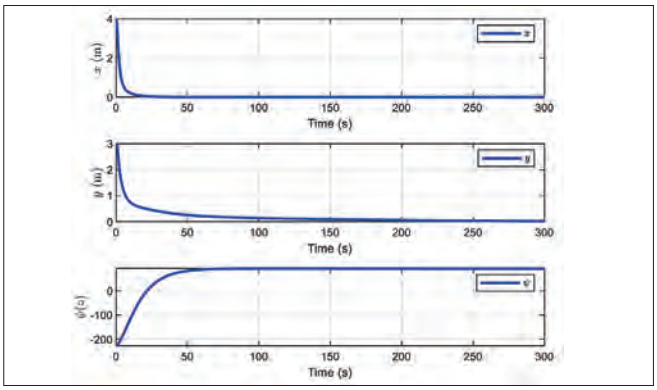

Fig. 2. Curves of the actual position and heading angle

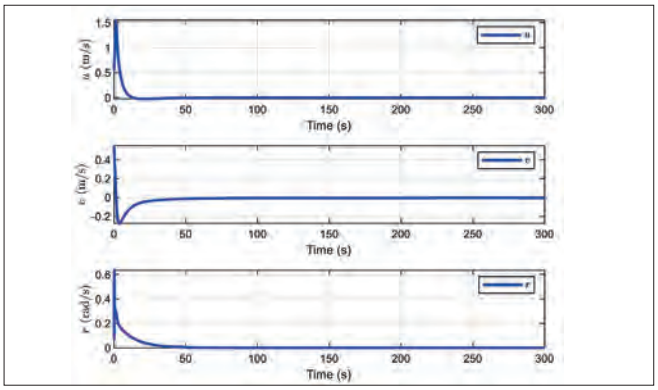

Fig. 3. Curves of the surge velocity u, sway velocity v and yaw rate r

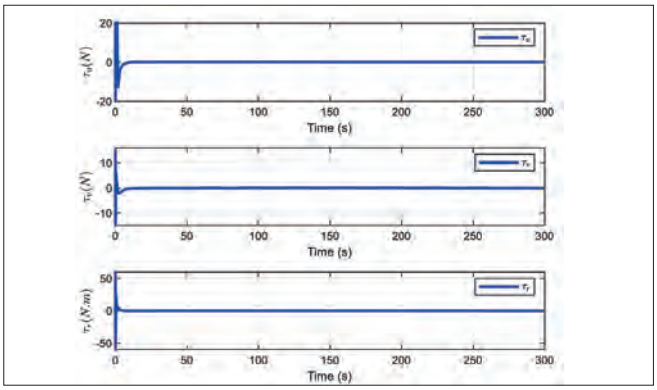

Fig. 4. Curves for the control input

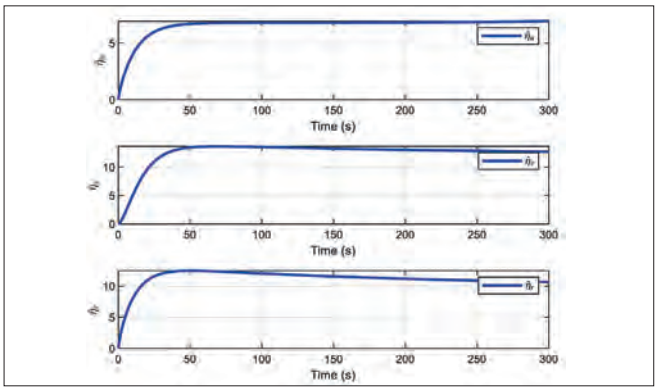

Fig. 5. Curves of $\hat{\eta}_u$, $\hat{\eta}_v$, $\hat{\eta}_r$

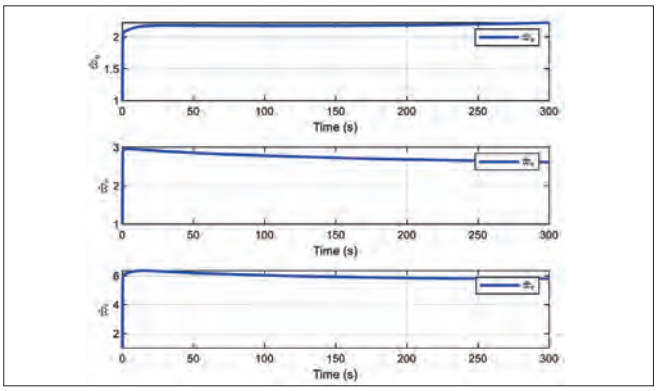

Fig. 6. Curves of $\hat{\bar{\omega}}_u$, $\hat{\bar{\omega}}_v$, $\hat{\bar{\omega}}_r$

system. Fig. 5 shows the dynamic changes in the LOE failure factor compensation process. Over time, this compensation mechanism effectively combats the adverse effects caused by LOE failures, which ensures safety during berthing. Fig. 6 shows the performance of the approximator in estimating uncertain dynamics. We can see that the approximator can accurately estimate the system dynamics under the influence of complex environmental factors, which further confirms the effectiveness of the proposed control scheme in handling uncertain dynamics. In summary, the MSV successfully completed the berthing task using the control scheme designed in this article.

CONCLUSION

In this paper, we have addressed the issue of the dynamics of internal and external uncertainties faced by vessels in port-restricted waters and the effects of actuator faults. We also developed and verified an efficient TBG-based finite-time fault-tolerant ABC scheme, in which RBFNNs were used to reconstruct the uncertainty dynamics accurately within the system, and MLP was used to transform the system's internal and external deterministic dynamics and bias faults into a neural single-parameter learning model. Subsequently, a robust adaptive technique incorporating depth information was used to establish an online approximator to estimate an upper bound consistent with uncertain dynamics. Through the use of DSC technology, the complexity of the virtual control derivative calculation was reduced. A predetermined finite time function based on time TBG ensured the finite time convergence of the system. Finally, we verified the effectiveness of the control scheme through simulation experiments. The proposed control scheme was found to meet the requirements for accurate berthing under the influence of actuator faults and uncertain dynamics.

FUNDING

This work was supported by the Education and Research Project for Middle and Young Teachers in Fujian Province (No: JAT210241).

REFERENCES

1. Shimizu S, Nishihara K, Miyauchi Y, et al. Automatic berthing using supervised learning and reinforcement learning. Ocean Engineering 265, 2022, doi: 10.1016/j.oceaneng.2022.112553.

2. Sun T, Yin Y, Liu C. Integrated trajectory planning into automatic berthing control of underactuated ship based on fuzzy-backstepping method. Ocean Engineering, 291, 2024, doi: 10.1016/j.oceaneng.2023.116336.

3. Zhang Y, Zhang M J, Zhang Q. Auto-berthing control of marine surface vehicle based on concise backstepping. IEEE Access 8:197059-197067, 2020, doi: 10.1109/ACCESS.2020.3034491.

4. Peng Z H, Wang C, Yin Y, et al. Safety-certified constrained control of maritime autonomous surface ships for automatic berthing. IEEE Transactions on Vehicular Technology 72(7):8541-8552, 2023.

5. Zhang Q, Zhu G, Hu X. Adaptive neural network auto-berthing control of marine ships. Ocean Engineering 177:40-48, 2019, doi: 10.1016/j.oceaneng.2019.02.031.

6. Xia G Q, Xue J J, Sun C, et al. Backstepping control using barrier Lyapunov function for dynamic positioning control system with passive observer. Mathematical Problems in Engineering 2019, doi: 10.1155/2019/8709369.

7. Yang H L, Deng F, He Y, et al. Robust nonlinear model predictive control for reference tracking of dynamic positioning ships based on nonlinear disturbance observer. Ocean Engineering 215, 2020, doi: 10.1016/j.oceaneng.2020.107885.

8. Meng X F, Zhang G C, Zhang Q, Han B. Event-triggered adaptive command filtered trajectory tracking control for underactuated surface vessels based on multivariate finite-time disturbance observer under actuator faults and input saturation. Transactions of the Institute of Measurement and Control, 2023, doi: 10.1177/01423312231195657.

9. Yu S L, Lu J S, Zhu G B, Yang SJ. Event-triggered finite-time tracking control of underactuated MSVs based on neural network disturbance observer. Ocean Engineering 253, 2022, doi:10.1016/j.oceaneng.2022.111169.

10. Zhu G B, Ma Y, Hu S L. Single-parameter-learning-based finite-time tracking control of underactuated MSVs under input saturation. Control Engineering Practice 105, 2020, doi:10.1016/j.conengprac.2020.104652.

11. Zhang Q, Zhang M J, Yang R M, et al. Adaptive neural finite-time trajectory tracking control of MSVs subject to uncertainties. International Journal of Control Automation and Systems 19(6):2238-2250, 2019.

12. Meng X F, Zhang G C, Zhang Q. Robust adaptive neural network integrated fault-tolerant control for underactuated surface vessels with finite-time convergence and event-triggered inputs. Mathematical Biosciences and Engineering 20(2):2131-2156, 2023, doi:10.3934/mbe.2023099.

13. Deng Y J, Zhang X K, Im N, Zhang G Q, Zhang Q. Model-based event-triggered tracking control of underactuated surface vessels with minimum learning parameters. IEEE Transactions on Neural Networks and Learning Systems 31(10):4001-4014, 2020, doi:10.1109/TNNLS.2019.2951709.

14. Ma Y, Zhu G B, Li Z X. Error-driven-based nonlinear feedback recursive design for adaptive NN trajectory tracking control of surface ships with input saturation. IEEE Intelligent Transportation Systems Magazine 11(2):17-28, 2019, doi: 10.1109/MITS.2019.2903517.

15. Zhu G B, Ma Y, Hu S L. Event-triggered adaptive PID fault-tolerant control of underactuated ASVS under saturation constraint. IEEE Transactions on Systems Man Cybernetics-Systems 53(8):4922-4933, 2023, doi:10.1109/TSMC.2023.3256538.

16. Meng X F, Zhang G C, Han B. Fault-tolerant control of underactuated MSVs based on neural finite-time disturbance observer: An event-triggered mechanism. Journal of the Franklin Institute 361(4), 2024, doi: 10.1016/j.jfranklin.2024.01.004.

17. Meng X F, Zhang G C, Zhang Q. Event-triggered trajectory tracking control of underactuated surface vessels with performance-improving mechanisms under input saturation and actuator faults. Transactions of the Institute of Measurement and Control 2023, doi:10.1177/01423312231187008.

18. Fossen T I. Handbook of marine craft hydrodynamics and motion control. Wiley; 2011.

19. Zhao K, Song Y, Wang Y. Regular error feedback based adaptive practical prescribed time tracking control of normal-form nonaffine systems. Journal of the Franklin Institute 356(5):2759-2779, 2019.

20. Park B S, Kwon J W, Kim H. Neural network-based output feedback control for reference tracking of underactuated surface vessels. Automatica,77:353-359, 2017, doi: 10.1016/j.automatica.2016.11.024.